AIAA'86

AIAA Paper No. 86-0593

# LDV/Rayleigh Scattering Measurements To Study The Blowoff of Swirling Flames

V. Tangirala, R.H. Chen, and J.F. Driscoll

Department of Aerospace Engineering
University of Michigan, Ann Arbor MI. 48109

**AIAA 24th Aerospace Sciences Meeting**
January 6-9, 1986/Reno, Nevada

# LDV/RAYLEIGH SCATTERING MEASUREMENTS TO STUDY THE BLOWOFF OF SWIRLING FLAMES

R.H. Chen, V. Tangirala, J.F. Driscoll*
Department of Aerospace Engineering
University of Michigan
Ann Arbor MI 48109

## Abstract

The use of swirl to improve flame stability and shorten the length of a flame makes it possible to operate practical combustion devices at relatively high fuel flowrates. However, the eventual blowoff limits are of fundamental importance in the design of industrial burners and gas turbine combustors. Three blowoff limits were identified in the present study. The three limits correspond to a maximum fuel velocity, a maximum swirl velocity, and a minimum swirl number. To help explain the blowoff limits, contours of mean velocity, turbulence level, and gas temperature were measured in twelve slightly lifted flames. Non-intrusive LDV and Rayleigh scattering diagnostics were used. For comparison, a TEACH code was used to numerically simulate the flames.

Measurements show that blowoff due to excess fuel velocity occurred after the fuel jet penetrated and weakened the recirculation bubble, which occurred for a ratio of fuel jet velocity to air axial velocity of 1.6. Excessive swirl caused visible stretching and fragmentation of the flame and caused blowoff of lean flames. Heat release caused local acceleration near the recirculation zone edge, increasing the recirculation. For the present geometry, cold flows did not recirculate until the swirl number exceeded one yet flames had recirculation for swirl numbers as low as 0.25. Rich flames were more stable than lean flames.

## Introduction

The blowoff of non-premixed flames is of fundamental importance to the design of combustion systems, including industrial burners as well as gas turbine combustors. For example, flame blowout in turbofan engines occurs at high altitude when the chemical kinetics are slowed by the low operating pressure, and it can occur for large air mass flowrates in military maneuvers. In industrial burners, blowoff limits the burner design for which the heat release rate and flame length can be tailored for a particular application.

One of the critical factors that is believed to affect flame blowoff is the way in which the local velocity, temperature, and fuel-air contours overlap in space.[1,2,3] If one considers a non-premixed lifted flame which has considerable premixing of fues and air in the liftoff region, blowoff is believed to occur when the local gas velocity normal the the flame everywhere exceeds the local turbulent burning velocity(1,2,3). An understanding of blowoff is complicated because the velocity normal the flame surface depends of flame orientation, i.e. the contours of local fuel-air ratio, as well as the contours of local turbulence level. Further complications arise because the contours of velocity and fuel-air ratio can be significantly altered by the flame itself(4) so additional non-intrusive measurements of these contours in flames (and not just cold flows) are needed.

In spite of the complications, there has been considerable progress made in the understanding of the blowoff of a non-premixed jet flame, which can be considered a two step process. As fuel velocity increases, there is the initial liftoff of the non-premixed, highly stretched flame. The rim geometry and local velocity gradient in the wake of the rim are important. Such flames have been analyzed by Peters and Williams(5) and Takahashi, et. al.(6). The second step is the blowoff of the lifted flame, which has been analyzed by VanTiggelen(1), Kalghatgi(2), and Chatravarty, Lockwood, and Sinicropi(7) who assume that fuel and air premix in the liftoff zone. Eichhoff, Lenze and Leuckel (8) present experimental evidence that such premixing does in fact occur. In addition, the importance of the mixing time scale and reaction time scale has been shown by Broadwell, Dahm, and Mungal(9).

Swirl stabilized flames are of special interest because they offer the enhanced stability and residence time required in many practical applications. Blowoff limits of swirling flames have been made by Leuckel and Fricker (10,11), Rawe and Kremer (3), and Syred, Chigier and Beer (12), among others. Sufficient swirl creates a recirculation zone and thus a contour surface along which the axial velocity is zero, as shown in Fig. 1. The flow pattern in Fig.1 was deduced from measurements described below and from photographs of Ref. 4. Of critical importance is the observation that the zero axial velocity line can cross the dividing streamline (which encloses hot non-combustible products) and can extend upstream into the region where the fuel and air first mix. At axial location z in Fig. 1, there can be two radial locations of zero axial velocity but the fuel-air ratio may be appropriate to support a flame only at the outer location, as shown. In the present study, the stabilization point appears as a ring of flamelets which is lifted one to two centimeters above the fuel tube. This is consistent with Fig. 1.

In swirling flames there are many factors that could cause blowoff, i.e. cause the contours of zero axial velocity, fuel concentration, and air concentration not to overlap properly. For example, Rawe and Kremer (3) found that excessive swirl can impart centrifugal forces that force the

*Associate Professor, Member AIAA

fuel-air contours to move too far radially outward and thus eliminate the critical region of overlap shown in Fig. 1.

The purpose of the present program is to measure blowoff limits for some lifted, swirl-stabilized flames and to map out the overlapping contours of velocity, turbulence levels, temperatures, and fuel concentrations in the flames using non-intrusive laser diagnostics. The present paper reports on some findings that relate the blowoff limits to the large scale recirculating flow pattern measured with LDV and Rayleigh scattering diagnostics. A future paper is planned to describe the localized flow pattern near the stabilization point; it is planned to measure fuel concentrations using laser induced fluorescence from an iodine tracer gas.

## Experimental Arrangement

Swirl stabilized flames were studied using the apparatus of Fig. 2. The fuels used were either pure methane or hydrogen enriched methane. A .711 cm. diameter fuel tube is surrounded by a swirling air flow in a tube of throat diameter of 2.22 cm. The swirl number S is defined to be identical to the conventional definition (12); it is the total angular momentum per second passing through the throat, divided by the axial momentum per second times the throat radius. S is determined from the measured flowrates of axial air and tangential air (13). A quarl section having 60 degree divergence was used, as seen in Fig. 2. Photographs of the resulting flames are given in Ref. 4.

Velocities were measured using and LDV system with two Bragg cells operated at 35 and 40 Mhz. At each location, 4700 samples were taken. The Rayleigh scattering system to measure gas temperature is based of principles described by Dibble (14) and others (15,16). Temperatures were measured for a fuel that was 83% methane, 17% hydrogen by weight, for which the Rayleigh cross sections of fuel, products, and air are equal to within 2% so that measured light intensity is inversely proportional to gas temperature. A 5 watt argon laser was used with an f/2 collection lens and a 3 Angstrom interference filter to eliminate flame radiation (16). Spatial resolution was 0.2X0.2X1.0 mm. At each location 8000 twelve bit samples were collected at 7.5 Khz.

## Results

A photograph of a typical swirl flame ($S=1, \Phi_o = .67$) is shown in Fig. 3a. The fuel flow pattern is visualized in Fig. 3b; aluminum oxide particles were injected into the fuel flow only and were illuminated using a sheet of laser light. A blue filter was used to eliminate blackbody radiation from particles not in the laser sheet. The fuel flow in Fig. 3b is seen to look similar to that shown in Fig. 1; a central fuel jet distorts the shape of the central recirculation bubble but does not penetrate all the way through. The fuel then passes over the outside edge of the recirculation bubble where it burns.

All the flames studied were slightly lifted by 1-2 cm. (except for a few flames which were attached to the fuel tube rim when hydrogen enriched methane was used, as described below.) Blowoff limits for methane flames are plotted in Fig.4a. The dependent variable is the maximum fuel flowrate which is proportional to heat output (kJoules/hr.). Results of Fig. 4a are similar to those obtained by Leuckel and Fricker (10) in a full scale industrial burner having gas flowrates 200 times larger than the present research burner. Fig. 4a shows that for S=1, optimum operation is at an overall equivalence ratio $\Phi_o$ of 0.8. Conversely, if the desired $\Phi_o$ is 0.8, the optimum swirl number is 1 and any increase or decrease in swirl will be destabilizing. The zero swirl flames were unstable unless the coflowing air velocity was reduced, forcing $\Phi_o$ to increase. Fig.4a also shows that for high swirl, lean flames were not stable, as discussed below.

It was found that a more useful way to plot the blowoff limits was tokeep the air flowrate fixed and to vary the swirl and fuel flow. Fig.4b shows results for an air flow rate of .435 kg/min. The three sides to the shaded stable region of Fig. 4b correspond to three independent physical reasons for blowoff. The left side of the stable region represents blowoff due to excessive fuel velocity $U_F$ with respect to axial air velocity $U_A$ at the throat. Measurements below and previous work (10) indicate that when $U_F/U_A$ exceeds a critical value, the fuel jet penetrates and weakens the recirculation bubble. Fig. 4b shows that the left blowoff limit is curved such that flames with higher swirl are more stable and can withstand larger $U_F/U_A$ before blowoff. While $U_F/U_A$ is a suitable parameter for the present study, a more suitable parameter in general is the momentum ratio $\rho_F U_F / \rho_A U_A$ where $\rho_F$ is the fuel density and $\rho_A$ is the recirculated air density which depends on the adiabatic flame temperature of the fuel used. Blowoff due to excessive fuel velocity also can result from one other mechanism besides fuel jet penetration of the recirculation zone; if fuel submerges the zero axial velocity contour in Fig. 1, blowoff can occur.

The lower limit to the stable region of Fig.4b represents the minimum swirl number S to cause recirculation. The minimum S is typically 0.25 and it increases as the flame becomes leaner, especially for the case of no quarl. Lean flames require a larger swirl to induce recirculation because rich flames have more heat release and it is shown below that heat release increases recirculation (4).

The upper limit to the stable region in Fig.4b represents a maximum swirl velocity. The high swirl limit is believed to be due to two causes: the flame is stretched and fragmented in the tangential direction due to large $U_\theta$ velocity tangential to the flame, and the excessive centrifugal forces throw the air radially outward so that the stoichiometric contour no longer overlaps the zero axial velocity line (3). Near the blowoff limit, the flame is observed to be fragmented, sometimes only existing in one third of the circumference of the flow and spins violently about centerline. Lean flames are less stable, as seen by the slope of the upper blowoff limit in Fig.4b; if more fuel is added the flame sheet becomes continuous over the entire circumference, restoring stability.

To nondimensionalize and thus generalize the maximum swirl velocity limit, it is seen that the swirl number (which is proportional to $U_\theta/U_A$) is not appropriate. In Figs. 4b,c and d, when $1/\Phi_o$ is 3 for example, the maximum swirl velocity $U_\theta$

is 30 m/sec independent of the axial air velocity $U_A$. Furthermore, the maximum $U_\theta$ limit increases with the laminar burning speed, as shown by Fig.5a for which 8% hydrogen is added to the methane. Rawe and Kremer (3) present a dimensional analysis that suggests one way to generalize the maximum swirl limits. Another way that is used for stretched flames is the consider the inverse Damkohler number which is the reaction time divided by the mixing time and is given by $U_\theta/(S_L^2\, d/\alpha)$ where $S_L$ is the stoichiometric laminar flame speed and $\alpha$ is the thermal diffusivity. Thus it might be more appropriate to scale the maximum value of $U_\theta$ by $S_L^2\, d/\alpha$ but further research is required.

The addition of hydrogen to the methane fuel improves stability by increasing the maximum fuel velocity and maximum swirl velocity, as seen in Fig.5. The flames were observed to be attached to the fuel tube rim for stable conditions depicted in Fig. 5 for which $\phi_o \leq 0.3$ (lean flames); flames were lifted by 1 cm. for $\phi_o \geq 0.3$.

Figures 4 and 5 also show that the use of a quarl section improves stability by reducing the minimum swirl number required from above 1.0 (no quarl) to as low as 0.25 (with quarl). The quarl is also seen to allow for larger fuel jet velocities before blowoff. With no quarl, the swirling air flow sees a step discontinuity in area: centrifugal forces require the air to rapidly expand radially outward causing a rapid decrease in swirl velocity in the axial direction. The only destabilizing effect of the quarl is the reduction of the maximum swirl velocity shown in Figs. 4 and 5. This is because the quarl forces the local tangential velocity to remain large at the flame stabilization point; i.e. it prevents rapid decrease in tangential velocity in the axial direction.

To better understand the measured blowoff limits, the velocity field was mapped out for twelve flames to date. Some of the results are shown in Fig.6. LDV measurements were made on one side of centerline only but are plotted on both sides for better visualization. The cold flow does not recirculate for S=1 (case 6a) yet the corresponding flames for S=1 do have internal recirculation (6b-d). This shows that local heat released by the flame accelerates the gas near the recirculation zone edge thereby enhancing the recirculation. As the fuel velocity $U_F$ is increased, the fuel jet eventually penetrates through the recirculation zone when $U_F/U_A$ equals 1.6 as seen in Fig. 6d. Leuckel and Fricker (11) report a similar value of $U_F/U_A$ of 2.0 for jet penetration. Further increases in $U_F/U_A$ were found to weaken the recirculation zone, resulting in blowoff. For swirl numbers exceeding one, all the cold flows had recirculation.

Local contours of turbulence level $k^{1/2}/U_A$ are shown in Fig. 7 where k is $(u'^2+v'^2+w'^2)/2$ and $U_A$ is the throat axial velocity of 12.7 m/sec in this case. Turbulence levels in the flame were more than twice that of the cold flow and reached a maximum near the flame stabilization location. The velocity profiles of Fig.8 show that there can be two radial locations of zero velocity, as was depicted in Fig.1. It is noted that the tangential velocity near the zero axial velocity locations is relatively low, so that flame stretch may not be important for this particular flame (S=1, $\phi_o$=1).

The temperatures measured in selected flames are plotted in Fig. 9. The visible flame was observed to exist near the T=2000 K isotherm; the theoretical adiabatic flame temperature of the methane-hydrogen mixture is 2330K. The temperature profiles, when overlapped with the velocity profiles, show that significant gas expansion occurs near the edge of the recirculation zone. In addition, By comparing Fig. 9b with Fig.9a, it is seen that fuel jet penetration of the recirculation zone (Fig.6d) drastically changes the temperature pattern in the flame.

## Numerical Model of the Swirling Flames

At present there are serious questions whether or not k-ε models or even higher order closure models have any predictive capabilities in complex flows such as swirling flames. The authors cannot state a position until the evaluation of the experimental data and the numerical calculations has been completed. Some disturbing differences have been noted between the assumption of small scale mixing in nearly all models and the observed bimodal velocity PDF in the present experiment(4) which indicates that large scale mixing(due to precession, flame movement, and perhaps large vortices) is important. However, the predicted mean velocity patterns shown below appear to be reasonable, and only the "universal" empirical constants in the code have been used.

The numerical code used was a version of the TEACH code written by Gosman, et. al.(17). It had been developed for an axisymmetric, propane-air, bluff body combustor; the boundary conditions(i.e. geometry) and the fuel type were changed to match those of the present experiment. The inlet profiles of velocity and turbulence levels at the throat were set equal to the measured profiles. The Favre-averaged form of the following conservation equations were solved:continuity, three momentum equations, enthalpy, a conserved scalar, mass fraction of fuel, turbulent kinetic energy, and turbulent dissipation rate. Closure of the non-linear elliptic equations for high Reynolds numbers is achieved by using gradient diffusion approximations for the Reynolds stress by introducing an algebraic relation between eddy viscosity and k and ε. The chemical reaction is modelled by approximating the source term in the equation for the fuel mass fraction in the manner proposed by Magnussen, et.al.(18).

The solution procedure is based on the finite volume approach and a Bounded Skew Hybrid Differencing Scheme (BSHD). Pressure-velocity coupling is handled using a Pressure Implicit Split Operator algorithm (PISO). The grid used was 30 by 30 grid points.The quarl was simulated using a stair case approximation for the inclined walls; 139 grid points were located inside the quarl. The non-uniform grid had more points near the quarl and fewer downstream. The inlet velocity profile was set equal to that measured using a hot wire anemometer at the throat; also, the inlet pressure was set equal to that measured at the throat using wall pressure taps. The inlet value of the dissipation rate was specified using the standard method, i.e. it is estimated by using empirical relations developed for pipe flows and boundary layers. This approximation is of major concern, of course, when assessing the validity of such models. At the combustor outlet, the gradients of all quantities except axial velocity were set to zero. The gradient of axial velocity at the exit is inherently adjusted by the code in the normal fashion to satisfy overall conservation of mass. At the centerline, the gradient

of all quantities is set to zero. Along each rigid wall, the normal velocity, the pressure correction, and gradient of fuel mass fraction and the conserved scalar are set to zero. Velocity parallel to the wall, and k are specified using wall functions (19) which replace any attempts to resolve the velocity profile in the wall boundary layer, which is too costly. Similarly, the dissipation rate near the wall is specified using the assumption of local equilibrium (19); wall temperature also is prescribed.

In strongly swirling flames, the hydro-mechanical equations for $U_z, U_\theta, U_r, p', p'', k$ and $\epsilon$ are strongly coupled to the thermo-chemical equations for h, $m_f$ and conserved scalar f through the mean density and the turbulent viscosity. Convergence of the solution will not occur unless the inlet swirl is slowly introduced as the iterations proceed. Also, the convergence is accelerated if a known converged solution for some other condition is used as the initial condition to obtain a desired higher swirl solution. Heavy underrelaxation of the equations for mean density, fuel mass fraction, and conserved scalar was required. The fuel flowrate also was slowly increased during the iteration procedure to the desired value.

The convergence criteria used is the standard criteria which requires that the sum of normalized residuals be less than 0.001 times the inlet values of the corresponding flow quantities. Isothermal flows were found to converge in 500 iterations wheras reacting flows converged in 800-1200 iterations, with lean flames converging faster than rich flames. The corresponding computational times were 700 sec for isothermal flows and 1100-1600 sec for flames on an AMDAHL 5860. Final runs were made on an APOLLO-DN660 minicomputer which required 35sec per iteration.

## Numerical Results

The calculated velocity patterns for four cases are shown in Figs.11-14. The first major observation is that the model, using "universal" empirical constants, at least predicts some of the gross features of the flow. That is, it predicts that for S=1, cold flow, there is no recirculation yet for S=1, $\Phi_o$=0.5 and 0.67 there is recirculation, which agrees with the experiment. The code also predicts that S=2 cold flow will recirculate for this geometry, as observed in the experiment.

The predicted values of turbulence levels are shown in Fig.15 for one selected case. It is seen that the predicted turbulence level is less than half than the measured values. This difference is believed due to the observation(4) that large scale motions are a primary cause of turbulence, and these large scale motions are neglected in the numerical model. The model also seems to overpredict the width of the recirculation zone, which agrees with the results of Correa(20). The mean temperature profiles calculated for one case are shown in Fig. 16 and they differ from the measured profiles in that the calculated flame is wider than the actual flame. Profiles of the predicted mixing length are shown in Fig. 17. The contours of calculated local reaction rate are shown in Fig.18; this quantity is the source term in the equation for fuel mass fraction.

## Acknowledgment

This research was supported by Gas Research Institute Grant 5083-260-0875.

## References

1. Vanquickenbourne,L, and VanTiggelen, A, Comb. and Flame, 10,59, 1966.
2. Kalghatgi,G. Comb. Sci Tech. 41,17,1984.
3. Rawe,R.and Kremer, H. 18th Symp on Combustion, 1981.
4. Tangirala,V.,Chen, R.H., and Driscoll,J.F., submitted to Comb. Sci. and Tech.
5. Peters,N. and Williams,F.A.,AIAA J. 21,3,1983.
6. Takahashi,F., Mizomoto,M.Ikai,S. and Futaki,N.,20th Symp. on Combustion,1985.
7. Chakravarty, A. Lockwood,F.C., and Sinicropi,F., Comb. Sci and Tech. 42,67,1984.
8. Eickhoff,H., Lenze,B.,and Leuckel,W., 20th Symp. on Combustion,1985.
9. Broadwell,J.E.,Dahm,W.J.A.,and Mungal,M.G.,20th Symp. on Combustion,1985.
10. Leuckel,W.and Fricker,N.,J.Inst.Fuel,49,103,1976.
11. Leuckel,W.and Fricker,N.,J.Inst.Fuel,49,152,1976.
12. Syred,N.,Chigier,N.and Beer,J.M.,13th Symp. on Combustion, 1971.
13. Claypole,T.C.and Syred,N.,18th Symp. on Comb.,1981.
14. Dibble,R.W. and Hollenbach,R.E.,18th Symp. on Combustion,1971.
15. Driscoll,J.F.,Schefer,R.W.and Dibble,R.W.,19th Symp. on Combustion,1982.
16. Gulati,A,and Driscoll,J.F., to appear in Comb. Sci. and Tech.,1986.
17. Gosman,A.D.and Pun,W.M., Report HTS/74/2,Imperial College, London,1974.
18. Magnussen,B.F.and Hjertager,B.H., 16th Symp. on Combustion,1978.
19. Khalil,E.E., Modelling of Furnaces and Combustors, Ed. by Gupta,A.K.and Lilley,D.G.,Abacus Press,1982.
20. Correa,S.M., AIAA Journal 22,11,1984.

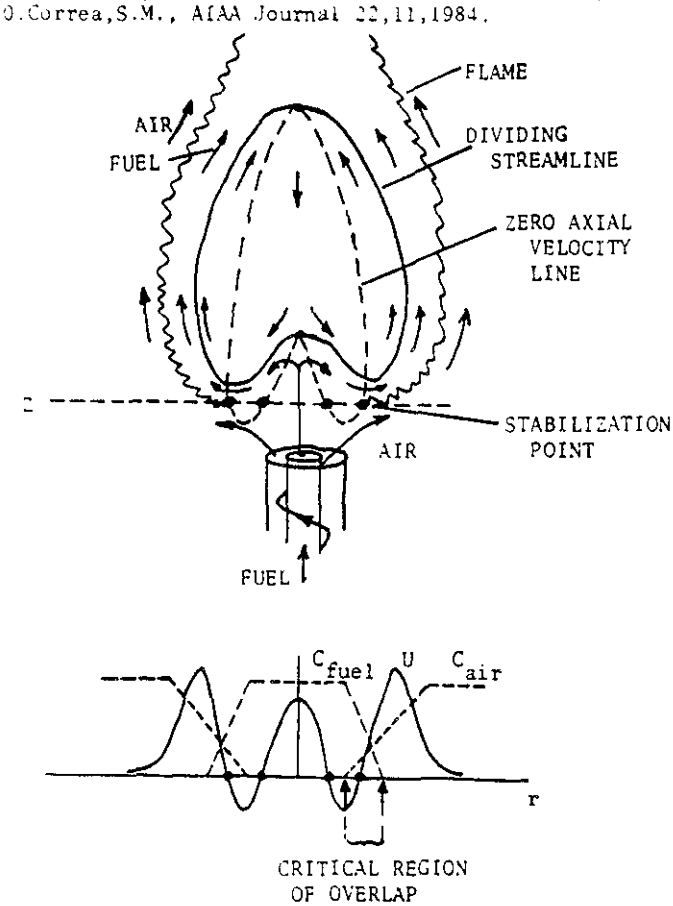


Figure 1. Schematic of Flame Stabilization Region

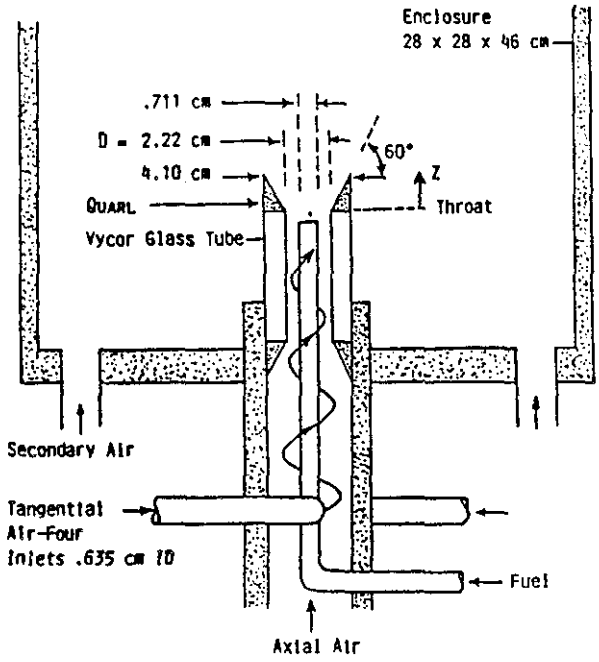


*Figure 2 Schematic of University of Michigan Swirl Burner*

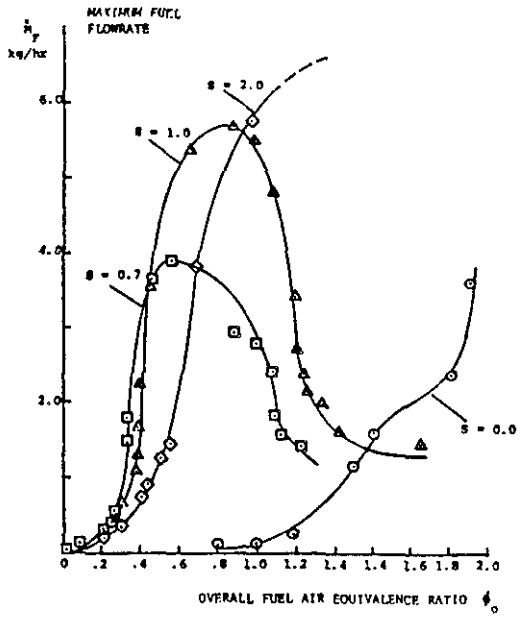


Figure 4a Maximum Fuel Flowrate at Blowoff for Various Swirl Numbers. Fuel = pure methane, quarl geometry same as Figure 1.

Figure 3. Photograph of swirl flame (S=1, $\phi_o$=0.67) and fuel flow visualization using alumina particles in fuel only

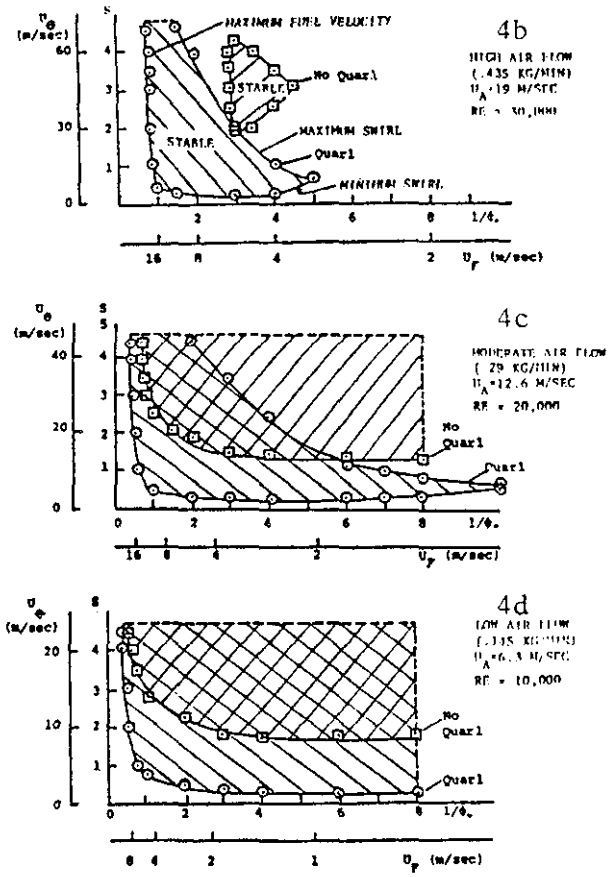


Flame Blowoff Limits for Methane, Geometry of Figure 2. Shaded Region = Stable Flame. $U_A$,$U_\theta$ = Axial air, Tangential air throat velocity $U_F$ = fuel exit velocity

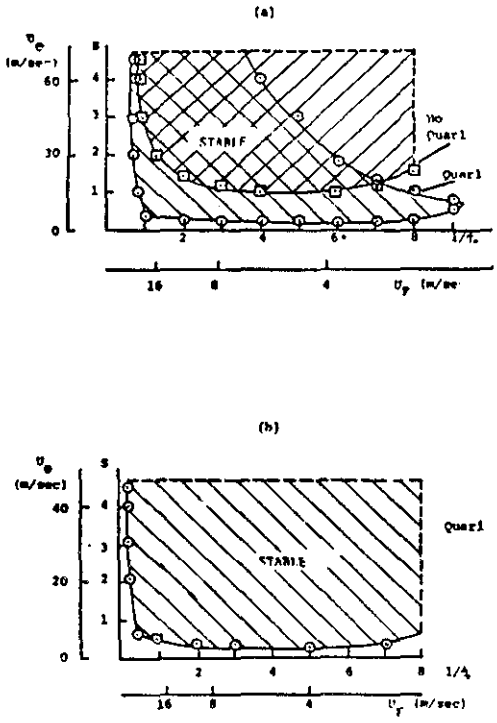


Figure 5. Flame Blowoff Limits For Hydrogen Enriched Methane Fuel. (a)= 8% hydrogen by weight added to case 4a; (b) = 17% hydrogen added to case 4b.

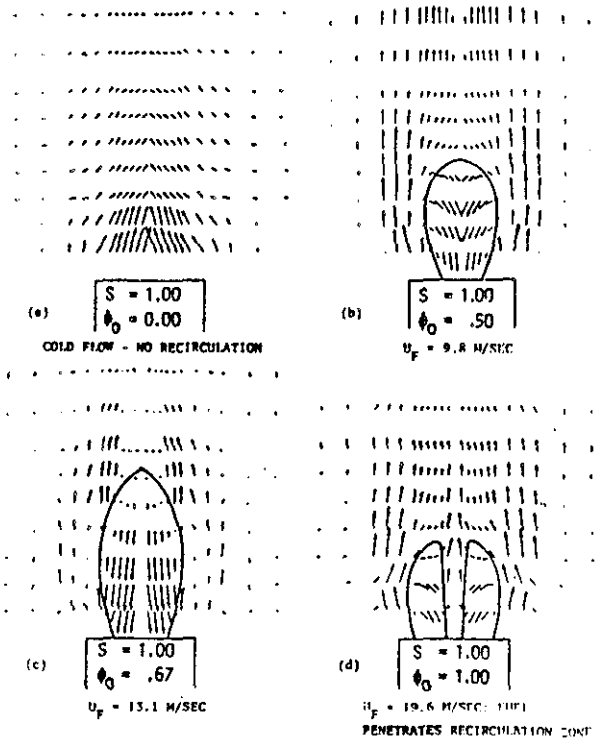


Figure 6. Measured Velocity Vectors in Flame and Cold Flow for S = 1.0 and Various Overall Equivalence Ratios $\phi_0$. Solid line is zero axial velocity line. Fuel = 83% Methane, 17% Hydrogen by weight, Geometry of Fig.2, Air flow = .29 kg/min, $U_A$ = 12.6 m/sec

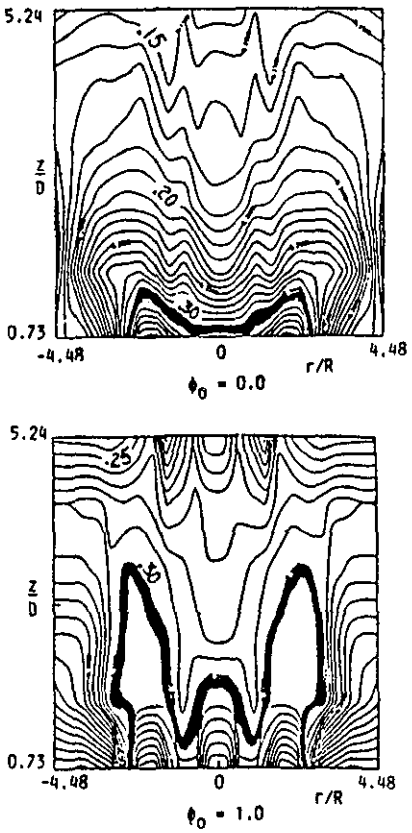


Figure 7. Contours of Turbulence Levels ($k^{\frac{1}{2}}/U_A$) For S = 1.0. Heavy line identifies region where $k^{\frac{1}{2}}/U_A$ exceeds 0.30. Flame conditions same as Figure 6.

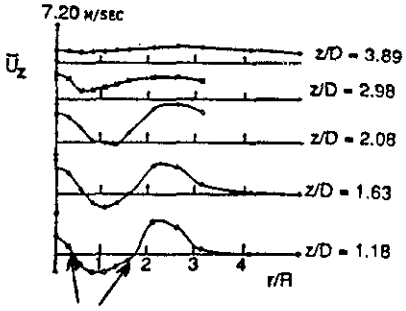


Zero axial velocity locations

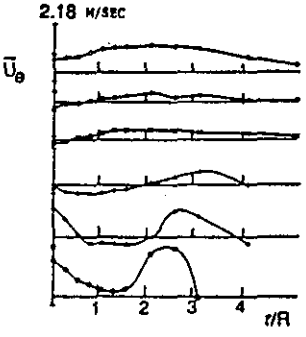


Figure 8a. Measured Velocity Profiles for Conditions of Figure 6, S-1, $\phi$=1.0; Fuel jet penetrates recirculation zone, note two locations of zero axial velocity as in Figure 1.

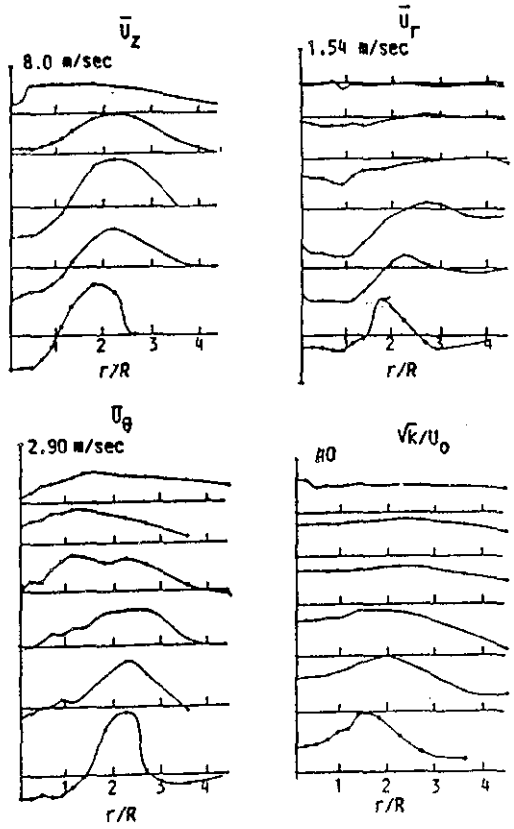


Figure 8b. Velocity and Turbulence Profiles Within Flame For $S = 1.0$, $\phi_o = 0.5$. ⊙: z/D = 1.18, Δ: z/D = 1.63, +: z/D = 2.08, x: z/D = 2.98, ◇: z/D = 3.89, †: z/D = 5.24.

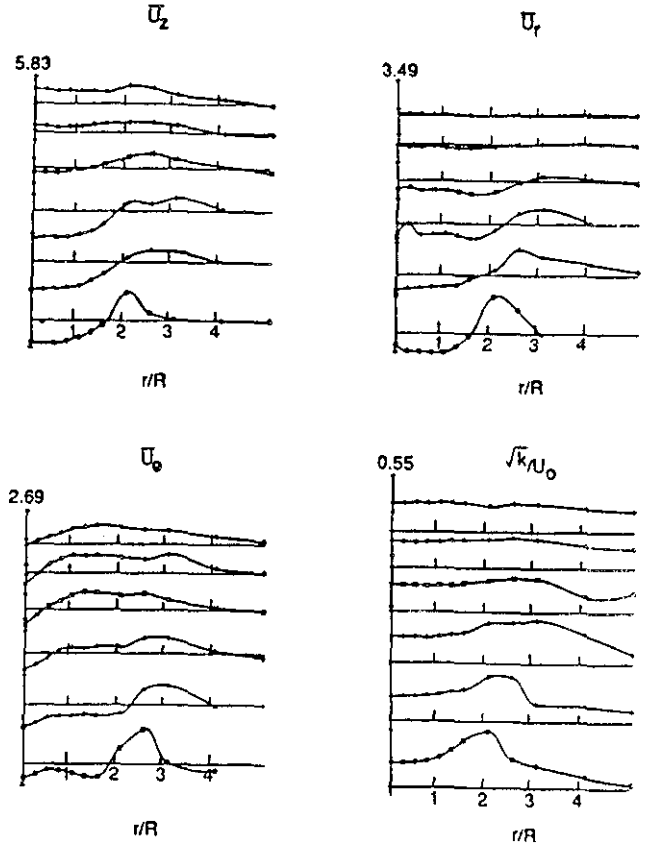


Figure 8c. Velocity and Turbulence Profiles Within Flame For $S = 2.0$, $\phi_o = 0.5$. ⊙: z/D = 1.18, Δ: z/D = 1.63, +: z/D = 2.08, x: z/D = 2.98, ◇: z/D = 3.89, †: z/D = 5.24

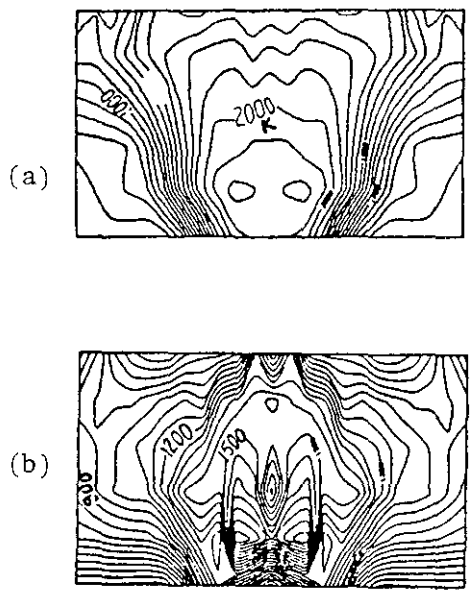


Figure 9. Measured Mean Temperatures in Kelvin Using Rayleigh Scattering; Conditions same as Figure 6: (a) no fuel jet penetration of recirculation zone, S=1, $\phi_o$=0.5; (b) fuel jet penetration, S=1, $\phi_o$=1.0.

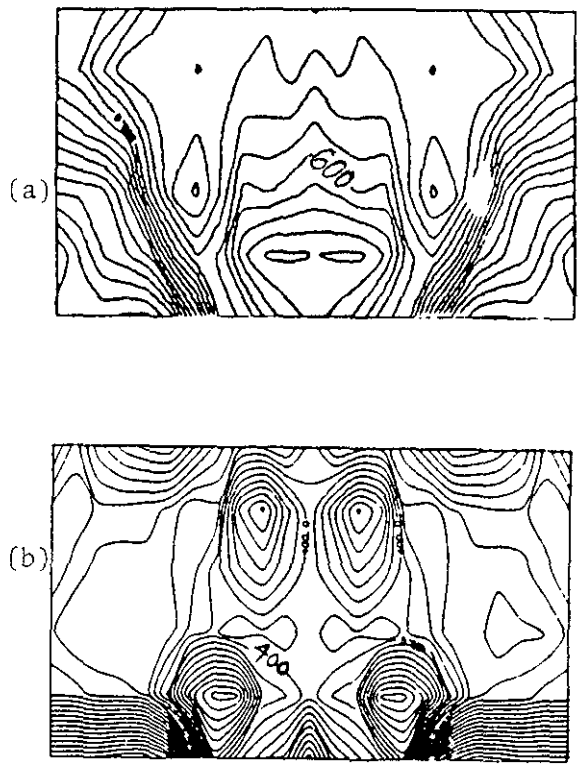


Fig. 10 Measured R.M.S. Temperature Fluctuations for conditions of Fig. 6b and 6d.

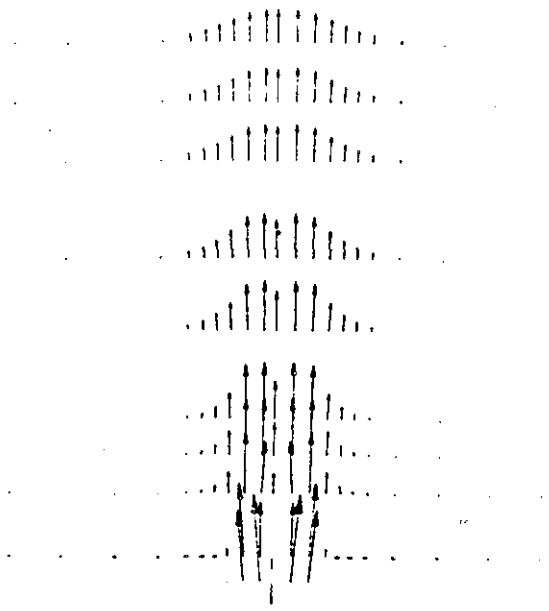

Figure 11. Calculated Velocity Field for S=1, cold flow

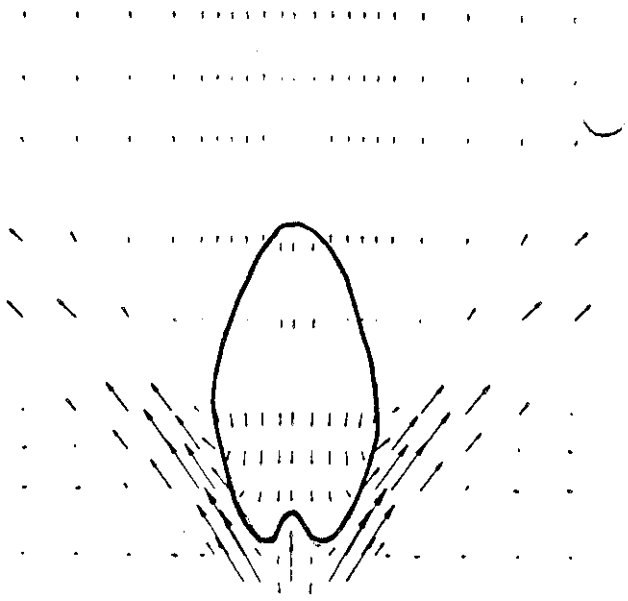

Figure 12. Calculated Velocity Field, S=1, $\phi_o$= 0.5

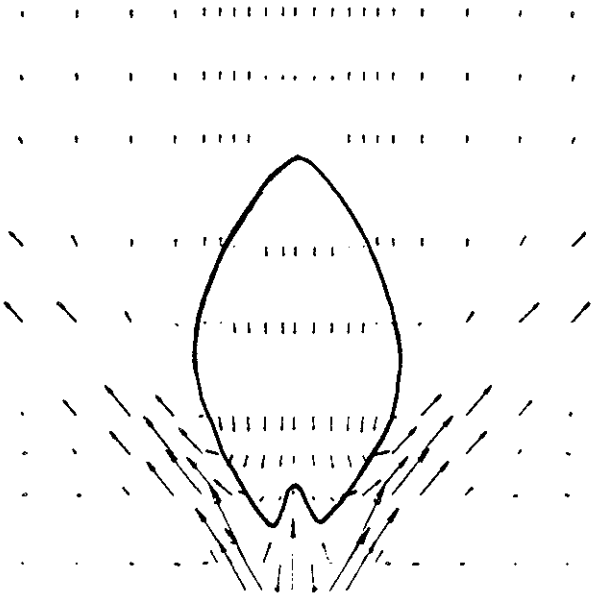

Figure 13. Calculated Velocity Field, S=1, $\phi_o$=0.67

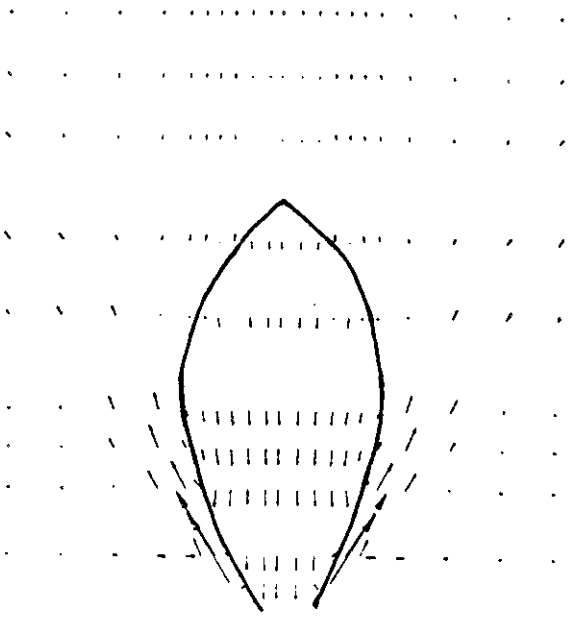

Figure 14. Calculated Velocity Field, S=2, $\phi_o$=0.0

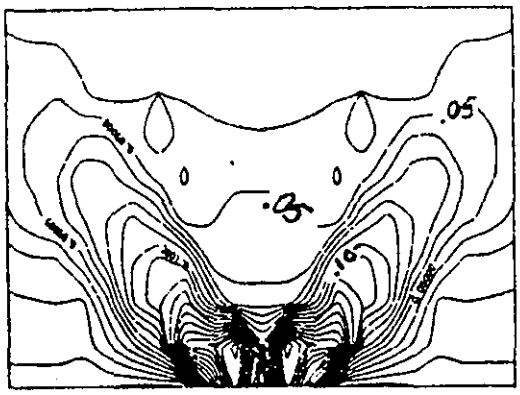


Figure 15. Calculated Turbulence Level $k^{1/2}/U_A$ for S=1, $\phi_o$=0.5

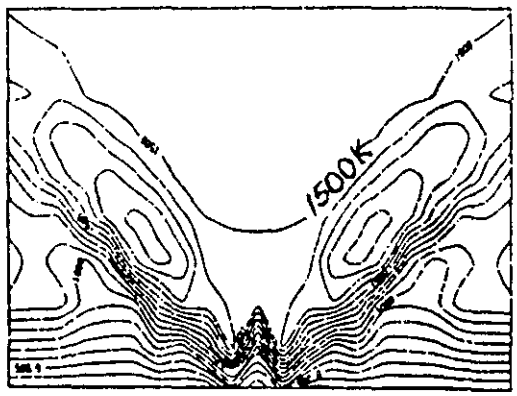


Figure 16. Calculated Mean Temperature for S=1, $\phi_o$=0.5

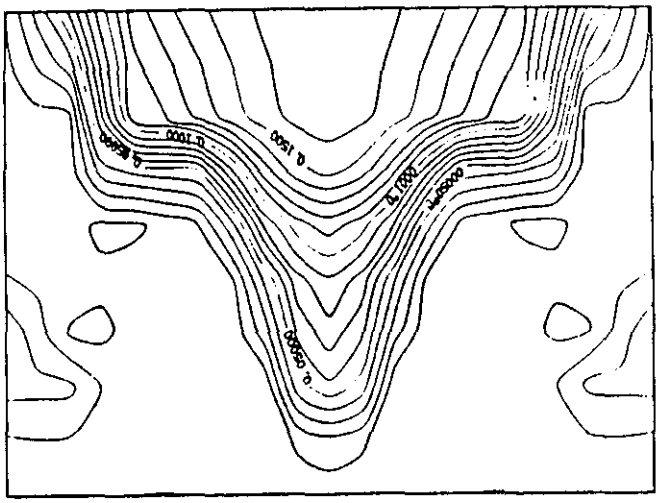

Figure 17. Calculated Mixing Length in meters for S=1, $\phi_o$=0.5

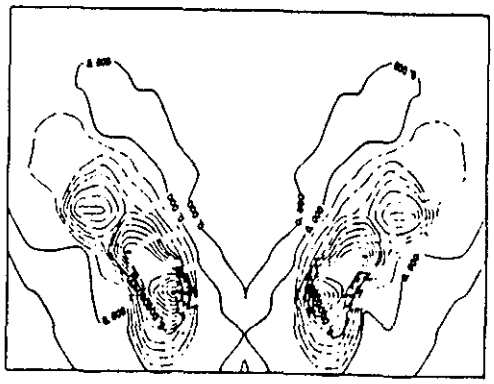

Figure 18. Calculated Profiles of Local Reaction Rate for S=1, $\phi_o$=0.5